JOURNAL OF MATERIALS SCIENCE 35 (2000) 981–987

Fracture behavior of calcium aluminate-phenol resin composite

G. K. D. PUSHPALAL
Maeta Techno-Research, Inc., 6-7 Kamihoncho, Sakata, Yamagata, 998-8611 Japan
E-mail: dinil.pushpalal@nifty.ne.jp

The strength and porosity relationship of very high strength cement based materials has been a famous research topic for many years. The author looks back on this relationship through the new class of macro-defect-free cement which is based on calcium aluminate cement and phenol resin. The flexural strength of this material is in the range of 120–200 MPa and has considerable stability to moisture and heat. The comparable composites made using alumina and aluminum hydroxide with phenol resin have given significantly lower strength, in spite of their low porous microstructure. Stress-deflection curves and scanning electron micrographs of the fracture surfaces of the composites revealed that the different fillers showed different behavior under load. The results demonstrated that the strong interparticle bonds created by the chemical interactions of the polymer and cement are significant in affecting the strength of calcium aluminate-phenol resin composite, whereas the alumina-phenol resin composite failed by debonding at the resin/filler weak interface.

1. Introduction

Macro-defect-free (MDF) cement has been a popular topic in cement researches in the 1980s. This was due to the unusual high bending strength. Whether this high strength was a result of reduced macro defects or enhanced chemical interaction between polymer and cement was a rigorous argument among the many articles which have been published in this journal and also others. The inventors of MDF cements [1, 2, 3] have attributed the high strength of the material to the elimination of critical flaws. This approach also implies that the polymer is used only as a rheological aid, to eliminate macro defects, and does not contribute to the properties of the material [3]. Several studies have looked at the fracture properties [4, 5] and chemical interactions of the material [6, 7]; and they have suggested that the polymer is more complex than that of an inert rheological aid.

A new class of MDF cement has been introduced by Kobayashi and coworkers [8, 9] at the beginning of this decade, which is based on calcium aluminate cement and phenol resin (this system, hereinafter is called the "CAPR composite"). In contrast to the previous MDF cement CAPR composite does not require any mixing water but contains 70 vol% of cement in the final material. However, the inventors have shown that cement utilizes water which is released by phenol resin during the methylene bridge formation reaction [10]. The flexural strength of the final product is in the range of 120–200 MPa and has considerable stability to moisture [11] and heat [12]. The specific properties of MDF cement and CAPR composite are briefly summarized in Table I.

Again, there is a continuing debate among the chemist and the fracture mechanist concerning the role of polymer and the porosity. Does cement work as a reactive filler? Does polymer work as a strong binder between cement particles? A basic aim of this paper is to identify the role of polymer and porosity in making high strength cement based material with a particular emphasis on those aspects which have been employed in studying the MDF cement system for over a decade. The chemical intimacy between calcium aluminate and phenol resin has been compared with inert fillers such as alumina and aluminum hydroxide, using fracture mechanics as the evaluation method.

2. Materials and mix proportions

2.1. Materials

2.1.1. Particulates

Commercially available high alumina cement, calcined alumina, and aluminum hydroxide were used in this study as particulates. High alumina cement used is composed of 54.3 wt% Al_2O_3, 37.0 wt% CaO, 4.5 wt% SiO_2 and 1.5 wt% Fe_2O_3. The main mineral constituent of high alumina cement is monocalcium aluminate (CA), but CA_2, $C_{12}A_7$, C_2AS and αAl_2O_3 are also identified by X-ray diffraction. Blaine specific surface area was 4750 cm^2/g, and specific gravity was 3.01. The particle size distribution of all the particulates was measured by a sedimentation technique on a granulometer (CILAS, Granulometer HR 850-B). The average particle size was 7 μm and the particle size distribution range was from 0.1 μm to 100 μm. Nearly equal quantities of particles between 1.5 μm and 48 μm were present without showing a sharp peak in the distribution pattern.

To study the effect of particle size on flexural strength, High Alumina Cement was separated into two

TABLE I The specific properties of the MDF cement and CAPR composite

	MDF cement	CAPR composite
Cement Type	Calcium aluminate	Calcium aluminate
Content (wt.%)	84.3	79.8
Binder Type	PVA	Phenol resin
Content (wt.%)	5.9	11.8
Solubility		
In water	Soluble	Insoluble
In alcohol	Insoluble	Soluble
Solvent	Water	Methanol
Processing promoter	Not necessary	Nylon

categories by using a classifier. The first category consisted of fine particles (median size of 1.6 μm) and the second consisted of coarse particles (median size of 16 μm).

Calcined alumina (specific gravity 3.94) was Alcoa A-10-325, which consisted of 99.7% α alumina. The median particle diameter of Alcoa A-10-325 was 8 μm and 95% of the particles were below 44 μm. Aluminum hydroxide (specific gravity 2.41) was Higilite HS-320 (manufactured by Showa Denko Co. Ltd.), and consisted of 99.9% $Al(OH)_3$. The median particle diameter was 5 μm and particles larger than 24 μm were not detected.

2.1.2. Organic components

Commercially available methanol soluble resole-type phenol resin precursor was used as the main binder. The precursor is essentially anhydrous and soluble in methanol, and contains 58 to 62 wt% of nonvolatile matter. Specific gravity is 1.09 and viscosity is 340 cps. N-methoxymethyl 6-nylon was incorporated to modify the phenol resin and to develop the plasticity of the paste. The chemistry of these two constituents has been given elsewhere [13]. Glycerol was used as a plasticizer.

2.2. Mix proportions

Seventeen types of mix proportions were used in this study and they are tabulated in Table II. All non-cement based mixtures (calcined alumina and aluminum hydroxide) were proportioned in consideration to differences of specific gravities; i.e. the total of particulate fillers in non-cement based mixtures is equal in volume to cement in appropriate mix proportion for cement (ex: total volume of Al_2O_3 and $Al(OH)_3$ in Mix No. 4-23 is equal in volume to cement in Mix No. 1-23). Mix No. 4-23 consisted of equal volume fractions of Al_2O_3 and $Al(OH)_3$. It should be noted that particle volume percentage in Table II was calculated by taking a ratio of the volume fraction of the particles in the initial composition to the volume fraction of the final material. It is assumed that only the solvent evaporates during processing and heat curing. Weighing the filler remaining after burning out the polymer revealed that the maximum possible error for the determination of filler volume fraction was 3%.

3. Methods

3.1. Preparation of specimens

The paste containing organic/inorganic components was prepared by mixing inorganic compounds, the modified methanol solution of phenol resin precursor, and plasticizer in a kneader-style mixer. This was followed by high shear mixing and calendering on a twin roll mill to form sheets. The resulting sheet can be cured at 200°C for 18 hours (Processing Route 1) or heat pressed under the pressure of 6 MPa at 80°C after calendering but before heat curing (Processing Route 2). Generally, 2.5 mm thick and 4.0–4.5 mm thick specimens were prepared. All the thicker specimens were prepared by route 2, unless otherwise stated. In order to prevent the sheets from squeezing out sideways, heat pressing was carried out after placing in a steel mold. Readers should refer elsewhere[12, 13] for more details of the method of processing.

TABLE II Mix proportions

				Mix proportions (parts by weight)						
				Particulates						
Mix no.	Particulates	Resin + Solvent + Modifier (parts by weight)	Particle volume (%)	HAC	Al_2O_3	$Al(OH)_3$	Resin	Solvent	Modifier	Plasticizer
1-40	HAC	40	58.14	100			22.70	14.33	2.96	4.0
1-36		36	60.68	100			20.43	12.90	2.67	3.6
1-32		32	63.46	100			18.16	11.47	2.37	3.2
1-30		30	64.94	100			17.03	10.75	2.22	3.0
1-26		26	68.13	100			14.76	9.32	1.93	2.6
1-23		23	70.73	100			13.05	8.24	1.70	2.3
1-20		20	73.53	100			11.35	7.17	1.48	2.0
2-48	Al_2O_3	48	53.65		131		27.24	17.20	3.56	4.8
2-42		42	56.95		131		23.84	15.05	3.11	4.2
2-40		40	58.14		131		22.70	14.33	2.96	4.0
2-36		36	60.68		131		20.43	12.90	2.67	3.6
2-30		30	64.94		131		17.03	10.75	2.22	3.0
2-26		26	68.13		131		14.76	9.32	1.93	2.6
2-22		22	71.64		131		12.49	7.88	1.63	2.2
3-26	$Al(OH)_3$	26	68.13			80	14.76	9.32	1.93	2.6
4-23	$Al_2O_3/Al(OH)_3$	23	70.73		66	40	13.05	8.24	1.70	2.3
5-26	HAC/Al_2O_3	26	68.13	50	66		14.76	9.32	1.93	2.6

In contrast to the HAC and $Al(OH)_3$ based pastes, calcined alumina based pastes could not be processed as a sheet. The reasons have been given elsewhere [10, 13, 14]. Therefore, after high shear mixing in the twin roll mill, alumina-phenol resin paste was packed into a steel mold and then heat pressed under 6 MPa at 165°C. The temperature was increased over three hours, culminating in a 30 min. treatment at 165°C. Samples were then heat cured in an oven and given a "final cure" for 18 h at 200°C. This resulted in a rigid material which was fairly free of voids and other adventitious flaws. The specimens prepared under this method ranged from 4.0 to 4.5 mm in thickness.

After the final heat curing, sheets were cut into 150 mm long and 10 mm wide strips by a water cooled diamond saw.

3.2. Measurements

Flexural strength and modulus were measured in a testing machine, following the guidelines set out in JIS K 6911 (Testing Methods for Thermosetting Plastics), which can be operated at a constant rate of crosshead motion. The specimens were subjected to a three-point bend test with the plate thickness as the beam depth. Flexural strengths were calculated from the load at failure and simple beam theory.

Deflection of the specimens was measured by a displacement transducer. Both load and deflection data were scanned into a computer, and modulus of elasticity was calculated from the slope of the load-deflection plot. The span to depth ratio was in all flexural strength tests in excess of 30 : 1 in order to ensure pure bending.

The pore structure of the samples was examined to understand the effect of porosity on strength. The optical microscopic photos of unfinished fracture surfaces were taken by a monitor microscope and scanned into a computer. Image processing was carried out by using Adobe Photo Shop Macintosh version, and the void area was measured. The maximum pore size was scaled by an image of an objective micrometer that was scanned into the computer. Also, pore volume and diameters were measured by mercury intrusion porosimetry (MIP).

For notched beam tests, 4.0 to 4.5 mm thick bars were used. Transverse notches of various depths were introduced into the tensile side of the beam using a water cooled fine diamond slitting saw, giving a slit of about 0.2 mm wide with a root radius of 100 μm. The specimens were tested in a three point flexure with a span of 50 mm at a crosshead speed of 1 mm/min. All strength tests were conducted at room temperature.

The fracture strength and notch depth relationship was discussed by using the Griffith equation

$$\sigma_n = (E\gamma/\pi c)^{1/2} \quad (1)$$

where σ_n is the flexural strength of the notched beam, γ is the fracture surface energy, c is the notch depth, and E is Young's modulus of elasticity. Equivalent crack length (a_e) was determined using the expression:

$$a_e = K_1^2/\sigma_n^2\pi \quad (2)$$

where K_1 and σ_n are the stress intensity factor and flexural strength of a beam for a given size of notch. The stress intensity factor for mode 1 opening, K_1, was measured under the guidance of JIS R 1607 (Testing Methods for Fracture Toughness of High Performance Ceramics).

4. Results and discussions

4.1. Effect of particle volume fraction

Fig. 1a and b show the effect of particle volume fraction on flexural strength and bending modulus, respectively. All the specimens were prepared according to mix proportions given in Table II and they were in the range of 4.0–4.5 mm in thickness. It can be seen from the plots in Fig. 1a that the HAC based composites (CAPR) have shown 2 times greater strength than alumina based composites for each particle volume fraction. The volume fraction of particles has a significant effect upon flexural strength, especially in HAC based composites. The strength is found to increase with an increasing volume fraction of particles up to a certain level and then tends to drop. The Young's modulus of HAC based

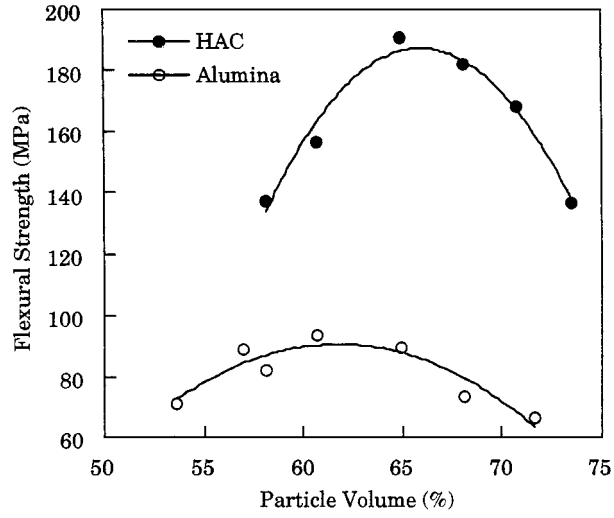

(a)

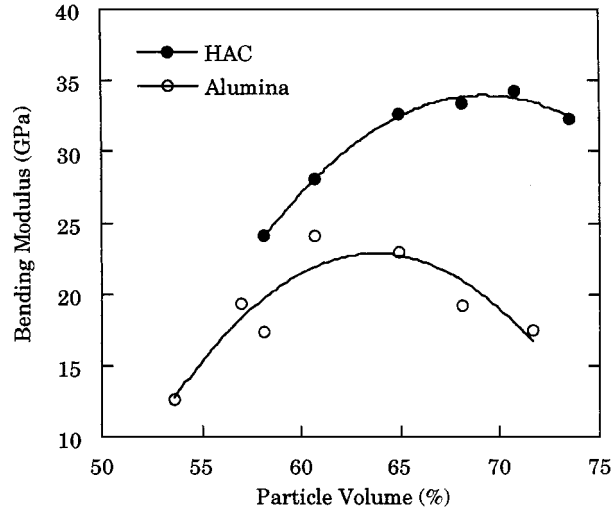

(b)

Figure 1 (a) The effect of particle volume fraction on flexural strength; (b) The effect of particle volume fraction on modulus.

composite (Fig. 1b) is found to increase, eventually levelling off with an increasing volume fraction of particles and dropping at 74% particle volume. These curves suggest that there is a minimum amount of resin required to lubricate the particles fully. In this specimen under these preparation conditions, that amount is about 11% for CAPR composites.

4.2. Stress-deflection curves

Stress-deflection curves for three materials which were prepared according to mix proportions 1-26, 2-26 and 3-26 are shown in Fig. 2 in an unnotched three point bend. All the specimens were in the range of 4.0–4.5 mm in thickness. It can be seen that the HAC based composite is completely brittle with a linear relationship between stress and deflection. The alumina based composite tends to obey Hooke's law at low deflections, and at high deflections is non-Hookean. Aluminum hydroxide shows a nearly linear relationship, but it is not completely elastic. It is interesting to consider the reasons for the differences between the three materials, and it is also worthwhile to consider the stress-deflection behavior of pure resin. Many polymers at low temperatures and high rates of strain display elastic behavior, whereas at high temperatures and low rates of strain they behave in a viscoelastic manner. However, Nelson and Turner [15] have shown that samples of resole-type phenol resin could be prepared which show little or no evidence of viscoelastic deformation in tensile stress-strain relationship, in contrast to many polymers. Thus, viscoelastic behavior shown by the non-cement based materials cannot be counted as a property related to the resin matrix. It must therefore be deduced that a mechanism like "debonding" at the filler matrix interface is occurring in the two non-cement based materials, and is even more pronounced in alumina.

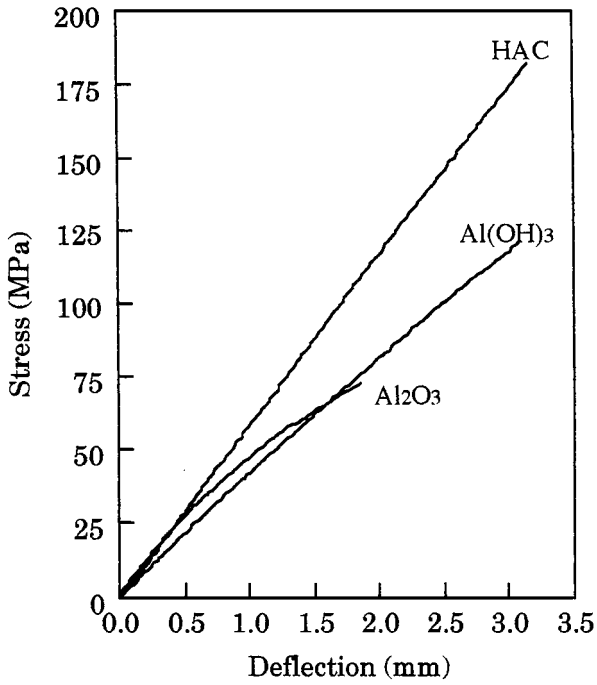

Figure 2 Stress-deflection curves for HAC, $Al(OH)_3$ and Al_2O_3 based composites.

4.3. Pore structure-strength relationship

The pore structure-strength relationship of filled phenol resin composites was investigated for some mix proportions and the results are shown in Table III. The specimens were prepared according to the mix proportions given in Table II. The structure-property relationship was investigated in 2.5 mm thick specimens and 4.0–4.5 mm thick specimens. Specimens were prepared using both processing routes (route 1 and 2) and the appropriate processing route is given in the Table III. As shown in the Table III, strength is heavily dependent on the processing route, specimen thickness, and particle size. Generally, detectable pores were not observed by graphical methods (Adobe Photo Shop) on the fracture surfaces of the specimens prepared by processing route 2.

Optical micrographs of fracture surfaces of No. 1, 4 and 9 are shown in Fig. 3. Fig. 3b is a computer scanned image of Fig. 3a, showing the distribution of flaws in the fracture surface. Comparatively higher strength was found for No. 4 specimens which consisted of the smallest particles, in spite of the existence of inherent crack-like pores (see Fig. 3c).

TABLE III Pore structure-strength relationship of filled phenol resin composites

							Pore structure		
No.	Mix type	Particle type	Particle size (μm)	Specimen thickness (mm)	Processing route	Strength (MPa)	Max. pore size (μm)	Pore area area (%)	Pore volume (%)
1	1-23	HAC	7	2.5	1	124	140	2.76	1.76
2	1-23		7	2.5	2	198	---	---	1.50
3	1-23		7	4.5	2	182	---	---	1.15
4	1-32		1.6	2.5	1	150	150	1.98	1.58
5	1-26		16	4.5	2	139	---	---	1.62
6	1-36		16	4.5	1	94	820		10.14
7	2-26	Al_2O_3	8	4.5	2[a]	73	---	---	2.80
8	3-26	$Al(OH)_3$	5	4.5	2	122	---	---	1.08
9	4-23	$Al(OH)_3/Al_2O_3$	5/8	2.5	1	95	80	1.32	1.12
10	5-26	HAC/Al_2O_3	7/8	2.5	1	100	170	1.80	1.20

---Detectable pores were not available.

[a]See Section 3.1 for the precise details of processing.

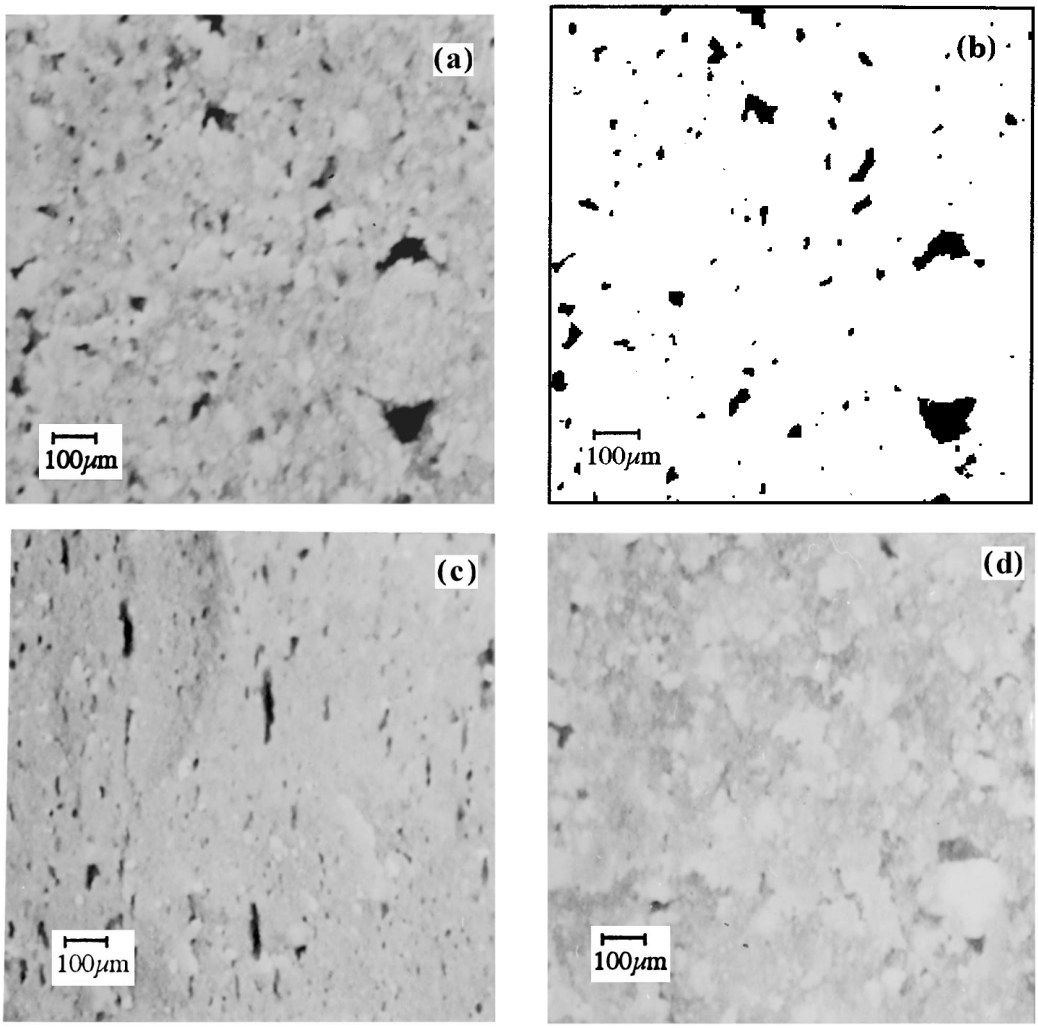

Figure 3 (a) Optical micrograph of fracture surface of No. 1; (b) Computer scanned image of (a), showing the distribution of flaws in the fracture surface; (c) & (d) Optical micrographs of fracture surfaces of specimens No. 4 & 9, respectively (magnification × 60).

In addition, No. 5 specimens which consisted of the largest particles have shown comparatively low strength, in spite of their low porosity. It suggests that the number of interparticle contacts decreased as particle size increased, hence simultaneously decreasing adhesion force at the contact points responsible for the lower strength. Another important observation in this study is that No. 6 specimens showed higher strength than No. 7, in spite of being large in pore size. Fig. 4 shows a scanning electron micrograph of the fracture surface of a No. 6 specimen. As shown in the figure, No. 6 specimens contain a lot of long pores which act as stress concentrators.

Fig. 5 shows the flexural strengths of notched beams as a function of the equivalent crack length (a_e) which were evaluated using No. 3 specimens. The results gave a reasonable fit to a straight line for notches exceeding 120 μm in length. For smaller notches than 120 μm, the strength was found to be nearly a constant. It was inferred that this deviation from the straight line was caused by the inherent flaws in the specimens which are larger than artificially introduced notches. It is interesting to note that No. 3 specimens contained considerably larger pores, though they were not detected by the optical microscopy and the accompanied evaluation method.

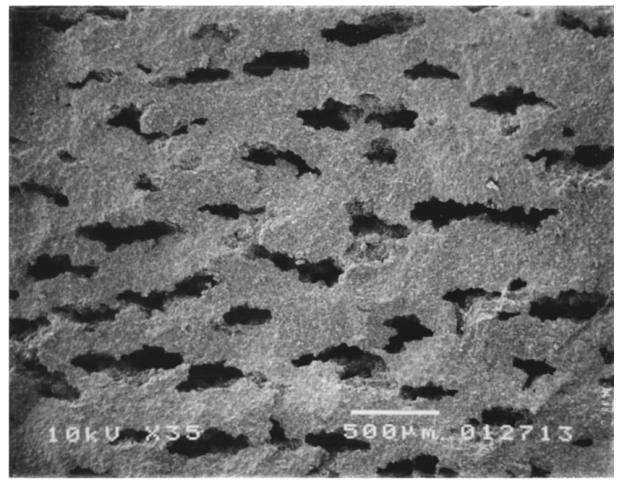

Figure 4 Scanning electron micrograph of fracture surface of a No. 6 specimen.

The lowest strength was found for No. 7 which consists of alumina particles, while aluminum hydroxide based material (No. 8) has shown moderate strength. These observations show that the high flexural strength of HAC based composite (CAPR) was due to a unique bonding between cement and phenol resin, while the low porosity of the material causes it to be stronger.

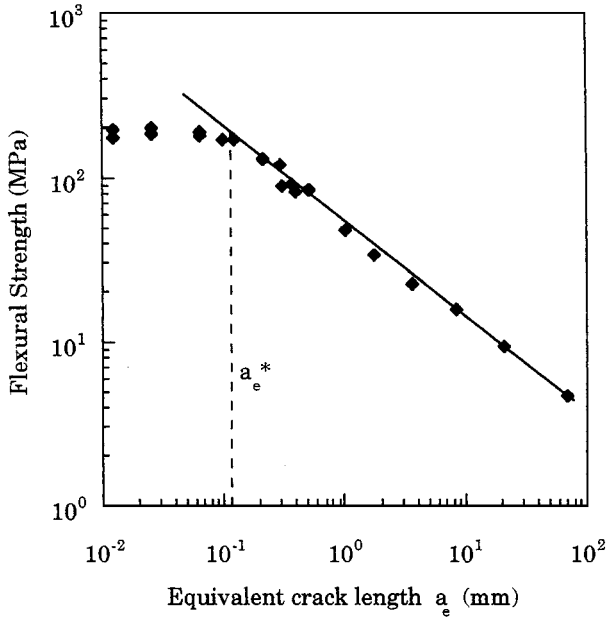

Figure 5 Flexural strengths of notched beams as a function of the equivalent crack length. Critical crack length (a_e^*) is 120 μm.

4.4. Applicability of Griffith criterion for phenol resin composites

The Griffith criterion of failure reveals that the strength of brittle materials increases with decreasing flaw size. In other words, the theory predicts that there should be a proportional relationship between the fracture strength and $c^{-1/2}$. To study the applicability of the Griffith theory to phenol resin composites, notched specimens of various depths were tested in a three point flexure. Fig. 6 shows the relationship between the fracture strength and $c^{-1/2}$ for HAC based composites. The specimens ranged from 4.0 to 4.5 mm in thickness. Only the strength/$c^{-1/2}$ relation of Mix types 1-40, and 1-30 were included in the figure, since they represent the lowest and the highest boundaries of the relationship. The results of other mix types were within the boundaries and have been omitted to prevent overcrowding. As shown in Fig. 6 there is a clear linear dependence of

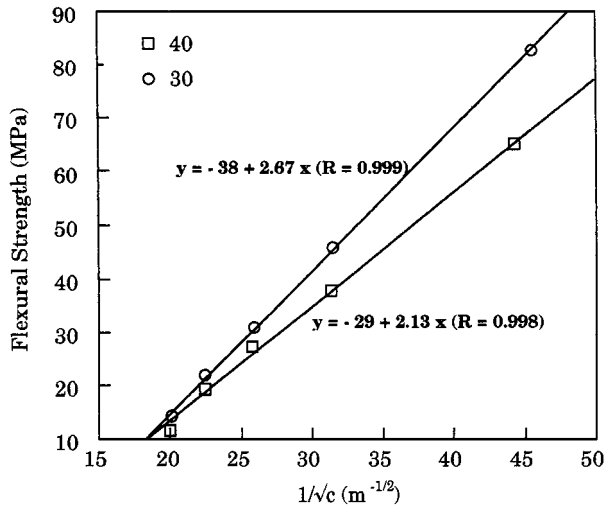

Figure 6 Relationship between the fracture strength and $c^{-1/2}$ for HAC based composites.

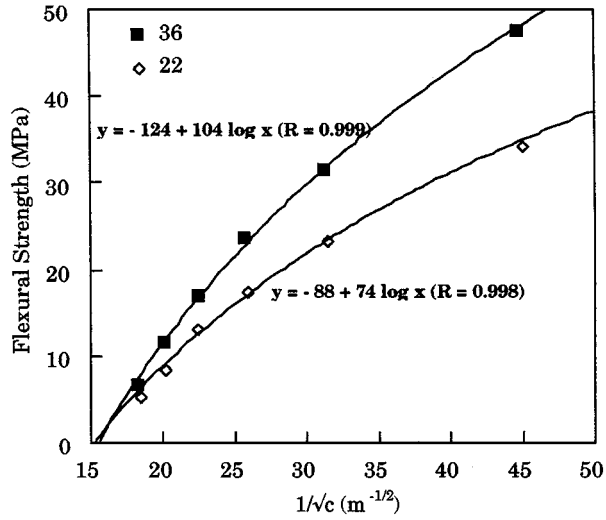

Figure 7 Relationship between the fracture strength and $c^{-1/2}$ for alumina based composites.

flexural strength upon $c^{-1/2}$ as predicted by the Griffith theory.

Fig. 7 shows the relationship between the fracture strength and $c^{-1/2}$ for alumina based phenol resin composites. The specimens were in the range of 4.0–4.5 mm in thickness. The results of Mix types 2-22 and 2-36 were included in the figure, which represent the lowest and the highest boundaries of the relationship. The most interesting aspects of these results are that the strength/$c^{-1/2}$ relationship of alumina composite shows a considerable degree of non-linearity and shows a logarithmic relation between strength and $c^{-1/2}$. Thus, it is apparent that Griffith's expression in the present form cannot be applied to alumina based composites.

Nelson and Turner [15] have examined the variation of fracture strength with the size of artificially introduced flaws for resole type phenol-formaldehyde resin. They found that fracture strength was linearly proportional to $c^{-1/2}$ as predicted by the Griffith equation. Thus, again, non-linearity showed by alumina based material cannot be accounted as a property related to resin matrix. As already pointed out in a previous section, this behavior is in marked contrast to HAC based composites, which supports our conclusions that the fracture behavior of the alumina based composite is different with CAPR, although both show catastrophic brittle fracture.

Fracture surfaces of CAPR composite and alumina based composite were examined by SEM. Figs 8 and 9 show the scanning electron micrographs of CAPR and alumina-phenol resin systems, respectively. The phenol resin in Fig. 8 formed a continuous matrix and fracture took place mainly through the polymer matrix. As shown in Fig. 9, the fracture path in the alumina-phenol resin system was through the grain-polymer interface, as shown clearly by the appearance of individual alumina grains on the fracture surface, indicating that the bonding between polymer matrix and grains is poor. This resulted in matrix filler debonding and the consequent lower flexural strength of the alumina-phenol resin system.

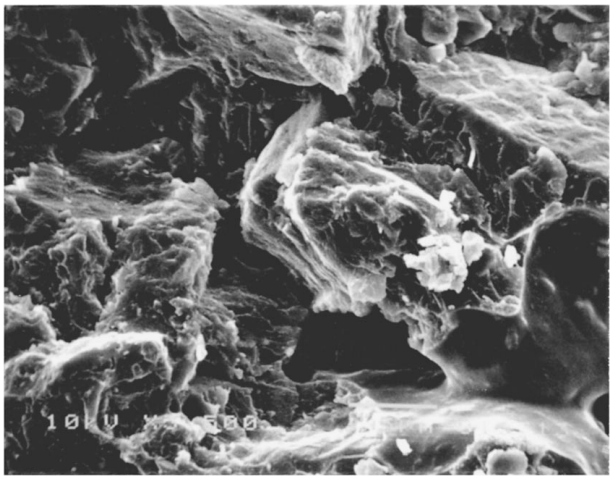

Figure 8 Fracture surface of CAPR composite showing fracture through polymer matrix.

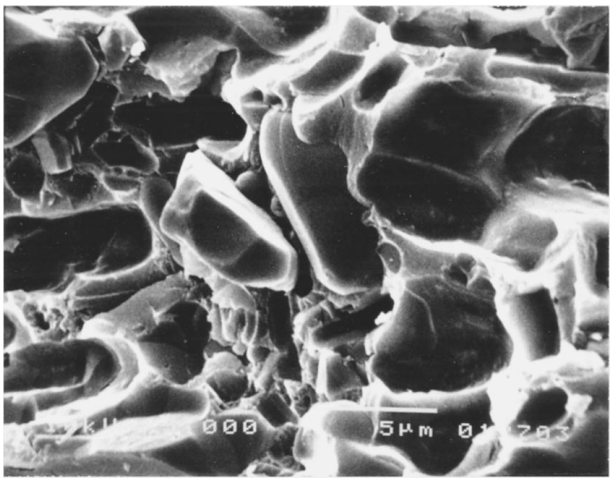

Figure 9 Fracture surface of alumina-phenol resin composite showing fracture through grain-polymer interface.

5. Conclusions

In this paper an attempt has been made to evaluate the fracture behavior of CAPR composite. The strong bonding phenomenon between calcium aluminate and phenol resin was compared with bonding of inert fillers such as alumina and aluminum hydroxide. CAPR composite has shown two times greater flexural strength than alumina based composites for each particle volume fraction tested. Alumina based composites showed non linear elastic behavior while CAPR was strictly linear. CAPR fits well into the Griffith curve, but alumina based composites showed a non-linear relationship between flexural strength and $c^{-1/2}$. This information is obviously of vital importance to the fracture process and it supports our conclusion that a mechanism like "debonding" at the filler matrix interface may be expected to occur in non-cement based materials. The high strength of CAPR cannot be simply accounted for by its low porosity since low porous non-cement based materials have given lower strengths. Thus the author has differentiated role of the calcium aluminate cement and alumina in the phenol resin matrix, in terms of their chemical nature [10].

Acknowledgements

The research work reported in this paper was carried out as the part of the author's Doctoral Dissertation in Toin University of Yokohama and was supported by the funds of Maeta Techno-Research, Inc. The author kindly appreciates the valuable advice and help of Prof. Masaki Hasegawa and Dr. Kiichi Tsuji during this investigation.

References

1. K. KENDALL, A. J. HOWARD and J. D. BIRCHALL, *Phil. Trans. R. Soc. Lond. A* **310** (1983) 139.
2. K. KENDALL and J. D. BIRCHALL, *Mater. Res. Soc. Symp. Proc.* **42** (1985) 143.
3. J. D. BIRCHALL, A. J. HOWARD and K. KENDALL, *Nature* **289** (1981) 388.
4. C. S. POON and G. W. GROVES, *J. Mater. Sci.* **22** (1987) 2148.
5. N. B. EDEN and J. E. BAILEY, *ibid.* **19** (1984) 2677.
6. R. N. EDMONDS and A. J. MAJUMDAR, *ibid.* **24** (1989) 3813.
7. S. A. RODGER, S. A. BROOKS, W. SINCLAIR, G. W. GROVES and D. D. DOUBLE, *ibid.* **20** (1985) 2853.
8. T. KOBAYASHI, G. K. D. PUSHPALAL and M. HASEGAWA, Japanese Patents to Maeta Concrete Industry Ltd., Japan. No. 2704925, No. 2704929, No. 2764684 (in Japanese).
9. *Idem.*, European Patent to Maeta Concrete Industry Ltd., Japan. No. 0590948 B1 (1997, priority date 29 September 1992); *Idem*., U.S. Patents to Maeta Concrete Industry Ltd., Japan. No. 5,609,680, No. 5,614,009, No. 5,651,816 (1997, priority date 21 December 1992).
10. G. K. D. PUSHPALAL, T. KAWANO, T. KOBAYASHI and M. HASEGAWA, *J. Adv. Cement-Based Mater.* **6** (1997) 45.
11. G. K. D. PUSHPALAL, T. KOBAYASHI and M. HASEGAWA, *Cem. Concr. Res.* **27** (1997) 1393.
12. G. K. D. PUSHPALAL, T. KOBAYASHI, T. KAWANO and N. MAEDA, *ibid.* **29** (1999) 121.
13. G. K. D. PUSHPALAL, Doctoral thesis, Toin University of Yokohama, 1997.
14. J. A. WALBERER and A. J. MCHUGH, *J. Adv. Cement-Based Mater* **8** (1998) 91.
15. B. E. NELSON and D. T. TURNER, *J. Polymer Sci.* **11** (1973) 1949.

Received 28 September 1998
and accepted 23 March 1999